Absorption of a rigid frame porous layer with periodic circular inclusions backed by a periodic grating

J.-P. Groby,[a] A. Duclos, and O. Dazel
Laboratoire d'Acoustique de l'Université du Maine, UMR6613 CNRS/Univ. du Maine, F-72085 Le Mans Cedex 9, France

L. Boeckx
Huntsman Europe, Everslaan 45, B-3078 Everberg, Belgium

W. Lauriks
Laboratory of Acoustics and Thermal Physics, KU Leuven, B-3001 Heverlee, Belgium

(Received 20 July 2010; revised 7 February 2011; accepted 13 February 2011)

The acoustic properties of a periodic rigid frame porous layer with multiple irregularities in the rigid backing and embedded rigid circular inclusions are investigated theoretically and numerically. The theoretical representation of the sound field in the structure is obtained using a combination of multipole method that accounts for the periodic inclusions and multi-modal method that accounts for the multiple irregularities of the rigid backing. The theoretical model is validated against a finite element method. The predictions show that the acoustic response of this structure exhibits quasi-total, high absorption peaks at low frequencies which are below the frequency of the quarter-wavelength resonance typical for a flat homogeneous porous layer backed by a rigid plate. This result is explained by excitation of additional modes in the porous layer and by a complex interaction between various acoustic modes. These modes relate to the resonances associated with the presence of a profiled rigid backing and rigid inclusions in the porous layer.
 [DOI: 10.1121/1.3561664]

PACS number(s): 43.55.Ev, 43.20.Fn, 43.20.Ks, 43.20.Gp [KVH] Pages: 3035–3046

I. INTRODUCTION

This work has been inspired by a problem that relates to the optimization of the profile of a layer of porous material for which the acoustic absorption coefficient needs to remain high across a broad frequency range. It is known that the acoustic absorption coefficient of a flat layer of a porous material of a finite thickness is high in the high frequency range but limited at the low frequencies. This problem is normally solved by multi-laying porous media to reduce the impedance mismatch at the air–material interface. The purpose of this article is to investigate an alternative to material multi-layering by studying the combined effects of embedding periodic rigid inclusions in a porous layer and by introducing periodic irregularities to the rigid backing on which the porous layer is rested.

The first effect has been previously investigated with the multipole method[1–3] which can account for the presence of rigid inclusions in a porous layer. If the radius of these periodic inclusions is comparable with the acoustic wavelength then an increase of the absorption coefficient mainly due to a decrease of the transmission coefficient in the case of one grating of inclusions or to band-gaps with total absorption peak in the case of a sonic crystal (multi-layered grating) can be observed. In the Refs. 1–3, the influence of the periodic inclusions on the absorption coefficient was explained by excitation of additional acoustic modes which dissipate acoustic energy due to the viscous and thermal effects in the material pores. When the porous layer is backed by a flat rigid surface and when only one inclusion per unit cell grating is embedded, an additional trapped mode can be excited. This results in a quasi-total absorption peak at a frequency below that of the usual quarter-wavelength resonance in the homogeneous layer case. Other studies related to volume heterogeneities in macroscopically homogeneous porous material were carried out essentially by means of homogenization procedure,[4,5] possibly leading to double porosity materials.[6]

The second effect was previously investigated by use of the multi-modal method in Ref. 7, by considering periodic rectangular air-filled irregularities of the rigid plate on which porous sheets are often attached. This leads, in the case of one irregularity per spatial period, to a total absorption peak associated with the excitation of the fundamental modified mode of the backed layer (MMBL). This mode is excited thanks to the surface grating. Such configurations have been widely studied in room acoustics whereby irregularities are introduced to the walls in a space to enhance the diffusion and absorption effects,[8] but the considered phenomenon are mostly related to resonance of the irregularities. Other works related to surface irregularities were carried out, notably related to local resonances associated with fractal irregularities.[9,10]

Local resonance and trapped modes[11–14] are other methods to localize the acoustic field thereby leading to an energy

[a]Author to whom correspondence should be addressed. Electronic mail: Jean-Philippe.Groby@univ-lemans.fr

entrapment and so to an increase of the absorption. In this article, the *combined effects* of embedding periodic circular inclusions inside a porous layer and of an irregular rigid backing attached to the back of the porous layer are investigated theoretically and numerically. The effect of the Bragg interference is clearly visible in the predicted absorption coefficient spectra. High peaks in the absorption coefficient spectra are obtained for frequencies close to or below the quarter-wavelength resonance in a hard-backed porous layer. These peaks are associated with the fundamental modified mode of the layer and with the trapped modes which are linked to the presence of the cylindrical inclusions and rectangular cavities in the irregular backing. Each of these modes interferes mutually.

II. FORMULATION OF THE PROBLEM

A. Description of the configuration

Both the incident plane acoustic wave and the geometry of the configuration are assumed to be invariant with respect to the Cartesian coordinate x_3. A cross-sectional x_1–x_2 plane view of the two-dimensional (2D) scattering problem is shown in Fig. 1.

Before the addition of the cylindric inclusions and of the structured backing, the layer is made of a porous material saturated by air (e.g., a foam), which is modeled (by homogenization) as a (macroscopically homogeneous) equivalent fluid $M^{[1]}$. The upper and lower flat and mutually parallel boundaries of the layer, whose x_2-coordinates are H and 0, are designated by Γ_H and Γ_0, respectively. $M^{[0]}$, the ambient fluid that occupies $\Omega^{[0]}$, and $M^{[1]}$ are in firm contact through Γ_H, i.e., the pressure and normal velocity are continuous across Γ_H ($[p(\mathbf{x})]=0$ and $[\rho^{-1}\partial_n p(\mathbf{x})]=0$, wherein ∂_n designates the operator $\partial_n=\mathbf{n}\cdot\nabla$, with $\mathbf{n}$ denoting the generic unit vector normal to a boundary). The spatial periodicity along x_1 is d.

N^c inclusions per spatial period are embedded in the porous layer that create a diffraction grating along the x_1 direction. Depending on the arrangement of the N^c inclusions in the unit cell, a diffraction grating or a sonic crystal of period d^c, $d^c \le d$ can be formed. The set of indices by which the cylinders within the unit cell are identified is denoted by $\mathcal{N}^c \in \mathbb{N}$. The jth inclusion occupies the disk $\Omega^{[2^{(j)}]}$ of radius $R^{(j)}$ and centered at $\mathbf{x}^{(j)}=(x_1^{(j)},x_2^{(j)})$, $j\in\mathcal{N}^c$. The inclusions are rigid (Neumann type boundary conditions on $\Gamma^{(j)}$, $\partial_n p(\mathbf{x})=0$), i.e., the contrast between the material that occupies the inclusions and $M^{[1]}$ is very large. This also means that the inclusions can consist in tubes or holes posteriorly proofed for acoustic waves. Two subspaces $\Omega^{[1^{\pm}]}\subset\Omega^{[1]}$ are also created respectively corresponding to the upper and lower part of the plate without inclusions.

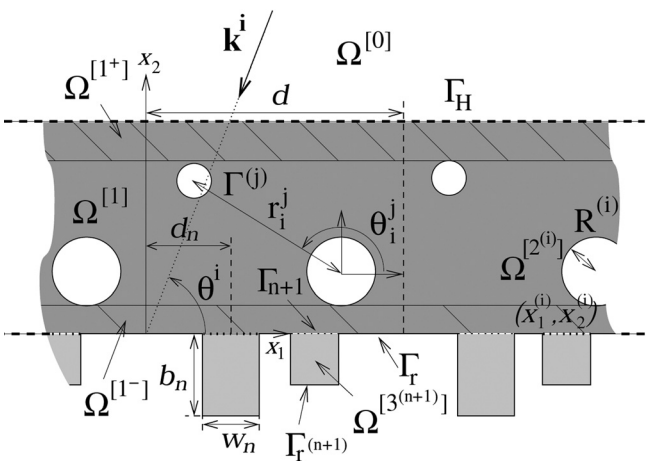

FIG. 1. Cross-sectional plane view of the configuration.

The rigid backing contains N^i rectangular irregularities per spatial period along the x_1 axis and creates a diffraction grating. In a similar way to the inclusions, a surface diffraction grating of periodicity d^i, $d^i \le d$, can be formed depending on the arrangement of the N^i irregularities in the unit cell. The set of indices by which the irregularities within the unit cell are identified is denoted by $\mathcal{N}^i \in \mathbb{N}$. The nth irregularity of the unit cell occupies the rectangular domain $\Omega^{[3^{(n)}]}$ of height b_n and width w_n and is occupied by a fluid material $M^{[3]}$ (in this study, $M^{[3]}$ is the air medium, but according to the formulation developed hereafter it can be any other fluid like material). The boundary of $\Omega^{[3^{(n)}]}$ is composed of the rigid portion $\Gamma_{r^{(n)}}$ (Neumann type boundary conditions) and of Γ_n, through which media $M^{[3]}$ and $M^{[1]}$ are in firm contact (continuity of the pressure and normal velocity). The x_1-coordinate of the center of the base segment of $\Omega^{[3^{(n)}]}$ is d_n. Γ_0 is also composed of a rigid portion Γ_r (Neumann type boundary conditions).

The total pressure, wavenumber, and wave speed are denoted by the generic symbols p, k, and c, respectively, with $p=p^{[0]}, k=k^{[0]}=\omega/c^{[0]}$ in $\Omega^{[0]}$, $p=p^{[1]}, k=k^{[1]}=\omega/c^{[1]}$ in $\Omega^{[1]}$, and $p=p^{[3^{(n)}]}, k=k^{[3]}=\omega/c^{[3]}$ in $\Omega^{[3^{(n)}]}$, wherein $\omega=2\pi\nu$ is the angular frequency with ν the frequency.

Rather than to solve directly for the pressure $\bar{p}(\mathbf{x},t)$ [with $\mathbf{x}=(x_1,x_2)$], we prefer to deal with $p(\mathbf{x},\omega)$, related to $\bar{p}(\mathbf{x},t)$ by the Fourier transform $\bar{p}(\mathbf{x},t)=\int_{-\infty}^{\infty} p(\mathbf{x},\omega)\, e^{-\mathrm{i}\omega t}d\omega$. Henceforth, we drop the ω in $p(\mathbf{x},\omega)$ so as to denote the latter by $p(\mathbf{x})$.

The wavevector $\mathbf{k}^{\mathbf{i}}$ of the incident plane wave lies in the sagittal plane, and the angle of incidence is θ^i, measured counterclockwise from the positive x_1 axis. The incident wave propagates in $\Omega^{[0]}$ and is expressed by $p^i(\mathbf{x})=A^i e^{\mathrm{i}(k_1^i x_1 - k_2^{[0]i}(x_2-H))}$, wherein $k_1^i=-k^{[0]}\cos\theta^i$, $k_2^{[0]i}=k^{[0]}\sin\theta^i$, and $A^i=A^i(\omega)$ is the signal spectrum.

The plane wave nature of the incident wave and the periodic nature of both $\bigcup_{j\in\mathcal{N}^c}\Omega^{[2^{(j)}]}$ and $\bigcup_{n\in\mathcal{N}^i}\Omega^{[3^{(n)}]}$ imply the Floquet relation

$$p(x_1+qd,x_2)=p(x_1,x_2)e^{\mathrm{i}k_1^i qd};\ \forall\mathbf{x}\in\mathbb{R}^2;\ \forall q\in\mathbb{Z}. \quad (1)$$

Consequently, it suffices to examine the field in the central cell of the plate in order to obtain the fields, via the Floquet relation, in the other cells.

The uniqueness of the solution to the forward-scattering problem is assured by the radiation conditions,

$$p^{[0]}(\mathbf{x})-p^i(\mathbf{x})\sim \text{outgoing waves};|\mathbf{x}|\to\infty,\ x_2>H. \quad (2)$$

B. Material modeling

Rigid frame porous material M is modeled using the Johnson–Champoux–Allard model. The compressibility and density linked to the sound speed through $c = \sqrt{1/(K\rho)}$ are[15,16]

$$\frac{1}{K} = \frac{\gamma P_0}{\phi\left(\gamma - (\gamma-1)\left(1 + \mathrm{i}\frac{\omega_c'}{\mathrm{Pr}\omega}G(\mathrm{Pr}\omega)\right)^{-1}\right)},$$
$$\rho = \frac{\rho_f \alpha_\infty}{\phi}\left(1 + \mathrm{i}\frac{\omega_c}{\omega}F(\omega)\right), \tag{3}$$

wherein $\omega_c = \sigma\phi/\rho_f\alpha_\infty$ is the Biot frequency, $\omega_c' = \sigma'\phi/\rho_f\alpha_\infty$, γ is the specific heat ratio, P_0 is the atmospheric pressure, Pr is the Prandtl number, ρ_f is the density of the fluid in the (interconnected) pores, ϕ is the porosity, α_∞ is the tortuosity, σ is the flow resistivity, and $\sigma\prime$ is the "thermal resistivity." The correction functions $G(\mathrm{Pr}\omega)$ (Ref. 17), $F(\omega)$ (Ref. 18) are given by

$$G(\mathrm{Pr}\omega) = \sqrt{1 - \mathrm{i}\eta\rho_f \mathrm{Pr}\omega\left(\frac{2\alpha_\infty}{\sigma\prime\phi\Lambda\prime}\right)^2},$$
$$F(\omega) = \sqrt{1 - \mathrm{i}\eta\rho_f\omega\left(\frac{2\alpha_\infty}{\sigma\phi\Lambda}\right)^2}, \tag{4}$$

where η is the viscosity of the fluid, $\Lambda\prime$ is the thermal characteristic length, and Λ is the viscous characteristic length. The thermal resistivity is related to the thermal characteristic length through $\sigma\prime = 8\alpha_\infty\eta/\phi\Lambda\prime^2$ (Ref. 17).

The configuration is more complex than those already studied in Refs. 1, 2, and 7 in the sense that it combines a rigid frame porous plate backed by a structured backing with a rigid frame porous plate in which inclusions are embedded. The method of solution is also briefly summarized emphasizing the differences in the coupling terms.

C. Field representations in $\Omega^{[0]}$, $\Omega^{[1^\pm]}$, and $\Omega^{[3^{(n)}]}$

The equations of continuity across the interfaces Γ_H and Γ_0 are first considered in Sec. III A. The field representations in $\Omega^{[0]}$, $\Omega^{[1^\pm]}$, and $\Omega^{[3^{(n)}]}$ are needed as the first step. The continuity conditions across $\Gamma^{(j)}$, $\forall j \in \mathcal{N}^c$ will be treated in Sec. III B.

Separation of variables, use of the radiation conditions, and application of the Floquet theorem lead to the representations

$$p^{[0]}(\mathbf{x}) = \sum_{q\in\mathbb{Z}}\left[e^{-\mathrm{i}k_{2q}^{[0]}(x_2-H)}\delta_q + R_q e^{\mathrm{i}k_{2q}^{[0]}(x_2-H)}\right]e^{\mathrm{i}k_{1q}x_1},$$
$$\forall \mathbf{x} \in \Omega^{[0]}, \tag{5}$$

wherein δ_q is the Kronecker symbol, $k_{1q} = k_1^i + 2q\pi/d$, $k_{2q}^{[0]} = \sqrt{(k^{[0]})^2 - (k_{1q})^2}$, with $\mathrm{Re}\left(k_{2q}^{[0]}\right) \geq 0$ and $\mathrm{Im}\left(k_{2q}^{[0]}\right) \geq 0$. R_q is the reflection coefficient of the plane wave denoted by the subscript q.

Referring to Refs. 7 and 19, the pressure fields $p^{[3^{(n)}]}$ admits the pseudo-modal representation that already accounts for the boundary conditions at $\Gamma_{r^{(n)}}$

$$p^{[3^{(n)}]}(\mathbf{x}) = \sum_{m=0}^{\infty} D_m^{(n)} \cos\left(k_{1m}^{[3^{(n)}]}(x_1 - d_n + w_n/2)\right)$$
$$\times \cos\left(k_{2m}^{[3^{(n)}]}(x_2 + b_n)\right), \forall \mathbf{x} \in \Omega^{[3^{(n)}]},$$
$$\forall n \in \mathcal{N}^i, \tag{6}$$

wherein $D_m^{[3^{(n)}]}$ are the coefficients of the pseudo-modal representation, $k_{1m}^{[3^{(n)}]} = m\pi/w_n$, and $k_{2m}^{[3^{(n)}]} = \sqrt{(k^{[3^{(n)}]})^2 - (k_{1m}^{[3^{(n)}]})^2}$, with $\mathrm{Re}\left(k_{2m}^{[3^{(n)}]}\right) \geq 0$ and $\mathrm{Im}\left(k_{2m}^{[3^{(n)}]}\right) \geq 0$, $\forall n \in \mathcal{N}^i$.

It is first convenient to use Cartesian coordinates (x_1, x_2) to write the field representations in $\Omega^{[1^\pm]}$. This field is composed of the diffracted field in the plate and of the fields scattered by the inclusions, whose form depends on the $\mathbf{x}$ position, either below or above the inclusions.[20] Referring to Ref. 1, whatever the arrangement of the inclusions, x_2 is always larger than $\max_{j\in\mathcal{N}^c}\left(x_2^{(j)} + R^{(j)}\right)$ in $\Omega^{[1^+]}$, while x_2 is always smaller than $\min_{j\in\mathcal{N}^c}\left(x_2^{(j)} - R^{(j)}\right)$ in $\Omega^{[1^-]}$. The total field in $\Omega^{[1^\pm]}$ can be written in Cartesian coordinates as[1,2]

$$p^{[1^\pm]}(\mathbf{x}) = \sum_{q\in\mathbb{Z}}\left(f_q e^{-\mathrm{i}k_{2q}^{[1]}x_2} + g_q e^{\mathrm{i}k_{2q}^{[1]}x_2}\right)e^{\mathrm{i}k_{1q}x_1}$$
$$+ \sum_{q\in\mathbb{Z}}\sum_{j\in\mathcal{N}^c}\sum_{l\in\mathbb{Z}} K_{ql}^{\pm} B_l^{(j)} e^{\mathrm{i}\left(k_{1q}\left(x_1 - x_1^{(j)}\right) \pm k_{2q}^{[1]}\left(x_2 - x_2^{(j)}\right)\right)}, \tag{7}$$

wherein $B_l^{(j)}$ are the coefficients of field scattered by the jth cylinder of the unit cell, f_q and g_q are the coefficients of the diffracted waves inside the layer associated with the plane wave denoted by q, and $K_{qm}^{\pm} = 2(-\mathrm{i})^m e^{\pm\mathrm{i}m\theta_q}/dk_{2q}^{[1]}$ with θ_q such that $k^{[1]}e^{\mathrm{i}\theta_q} = k_{1q} + \mathrm{i}k_{2q}^{[1]}$ (Refs. 20 and 21).

III. DETERMINATION OF THE ACOUSTIC PROPERTIES OF THE CONFIGURATION

A. Application of the continuity conditions across Γ_H and Γ_0

Applying the continuity of the pressure field and of the normal component of the velocity, together with Neumann type boundary conditions across Γ_H and across Γ_0, introducing the proper field representation therein, Eqs. (5), (6), and (7), and making use of the orthogonality relations $\int_{-d/2}^{d/2} e^{\mathrm{i}(k_{1n}-k_{1l})x_1}dx_1 = d\delta_{nl}$, $\forall (l,n) \in \mathbb{Z}^2$, and $\int_0^{w_n}\cos\left(k_{1m}^{[3]}x_1\right)\cos\left(k_{1q}^{[3]}x_1\right)dx_1 = w_n\delta_{mq}/\varepsilon_m$, wherein $\varepsilon_0 = 1$ and $\varepsilon_m = 2$, $\forall m \in \mathbb{N}^\star$, gives rise to a first linear set of equations. After some algebra and rearrangements, this linear set reduces to a first coupled system of equations for solution of $D_m^{(n)}$ and $B_l^{(j)}$, which may be written in the matrix form

$$(\mathcal{A} - \mathcal{C})\mathbf{D} - \mathcal{Z}\mathbf{B} = \mathcal{F}. \tag{8}$$

In the above expression, $\mathbf{D}$ and $\mathbf{B}$ are the infinite column matrices of components $D_m^{(n)}$ and $B_l^{(j)}$, respectively. $\mathcal{F}$ is the column matrix of elements $\sum_q \mathcal{F}_{qM}^{(N)}$, $\mathcal{A}$ is a diagonal square matrix of elements $\mathcal{A}_M^{(N)}$, and $\mathcal{C}$ and $\mathcal{Z}$ are two square matrices of elements $\sum_{q\in\mathbb{Z}} \mathcal{C}_{qMm}^{(N,n)}$ and $\sum_{q\in\mathbb{Z}} \mathcal{Z}_{qMl}^{(N,j)}$, respectively. These elements are:

$$\mathcal{F}_{qM}^{(N)} = \frac{2\alpha_q^{[0]}\delta_q}{D_q} I_{qM}^{+(N)} e^{\mathrm{i}k_{1q}(d_N - w_N/2)},$$

$$\mathcal{A}_M^{(N)} = \frac{1}{\varepsilon_M}\cos\left(k_{2M}^{[3^{(N)}]} b_N\right),$$

$$\mathcal{C}_{qMm}^{(N,n)} = \frac{\mathrm{i}w_n\alpha_m^{[3^{(n)}]}\left(\alpha_q^{[1]}\cos\left(k_{2q}^{[1]}H\right) - \mathrm{i}\alpha_q^{[0]}\sin\left(k_{2q}^{[1]}H\right)\right)}{dD_q\alpha_q^{[1]}} \sin\left(k_{2m}^{[3^{(n)}]} b_n\right) I_{qm}^{-(n)} I_{qM}^{+(N)} e^{\mathrm{i}k_{1q}((d_N - d_n) - (w_N - w_n)/2)},$$

$$\mathcal{Z}_{qMl}^{(N,j)} = \frac{4(-\mathrm{i})^l\left(\alpha_q^{[1]}\cos\left(k_{2q}^{[1]}\left(x_2^{(j)} - H\right) - l\theta_q\right) + \alpha_q^{[0]}\mathrm{i}\sin\left(k_{2q}^{[1]}\left(x_2^{(j)} - H\right) - l\theta_q\right)\right)}{dk_{2q}^{[1]}D_q} I_{qM}^{+(N)} e^{-\mathrm{i}k_{1q}x_1^{(j)}} e^{\mathrm{i}k_{1q}(d_N - w_N/2)},$$

$$D_q = \alpha_q^{[0]}\cos\left(k_{2q}^{[1]}H\right) - \mathrm{i}\alpha_q^{[1]}\sin\left(k_{2q}^{[1]}H\right),$$

$$I_{qm}^{\pm(n)} = \frac{e^{\pm\mathrm{i}k_{1q}\frac{w_n}{2}}}{2}\left(e^{\mathrm{i}k_{1m}^{[2^{(n)}]}\frac{w_n}{2}}\mathrm{sinc}\left(\left(k_{1m}^{[2^{(n)}]} \pm k_{1q}\right)\frac{w_n}{2}\right) + e^{-\mathrm{i}k_{1m}^{[2^{(n)}]}\frac{w_n}{2}}\mathrm{sinc}\left(\left(k_{1m}^{[2^{(n)}]} \mp k_{1q}\right)\frac{w_n}{2}\right)\right), \tag{9}$$

where $\mathrm{sinc}(\chi) = \sin(\chi)/\chi$, $\alpha_q^{[s]} = k_{2q}^{[s]}/\rho^{[s]}$, $s = 0,\ 1,$ and $\alpha_m^{[3^{(n)}]} = k_{2m}^{[3^{(n)}]}/\rho^{[3]}$. The components $\mathcal{F}_{qM}^{(N)}$ accounts for the excitation of the Nth irregularity by a wave that is previously diffracted by the layer. The components $\mathcal{A}_M^{(N)}$ and $\mathcal{C}_{qMm}^{(N,N)}$ account for the Nth irregularity, while the components $\mathcal{C}_{qMm}^{(N,n)}$, $n \neq N$, account for the coupling between the Nth and the nth irregularities through waves that are traveling inside the porous layer. These components are those found in Ref. 7 in which a rigid frame porous layer backed by a multi-component grating is considered. The components $\mathcal{Z}_{qMl}^{(N,j)}$ account for the coupling between the Nth irregularity and the jth circular inclusion through waves that are traveling through the porous layer.

B. Application of the multipole method

From the first linear set of equations, obtained by applying the continuity conditions across Γ_H and Γ_0, expressions of R_q, f_q, and g_q in terms of $D_m^{(n)}$ and $B_m^{(j)}$ can be found.

In particular, the expressions of f_q and g_q are introduced in the so-denoted diffracted field inside the layer. This field accounts for the direct diffracted waves inside the layer and for the reflected waves at the boundaries Γ_H and Γ_0 previously scattered by each inclusion. This expression, when compared with the expression of the direct scattered field by the inclusions, is valid in the whole domain $\Omega^{[1]}$. To proceed further, the Cartesian form of this field is converted to the cylindrical harmonic form in the polar coordinate system attached to each inclusion, as stated for example in Ref. 1. Effectively, central to the multipole method is the local field expansion or multipole expansions around each inclusion. The difference here, when compared with Refs. 1 and 2 is that more than one inclusion per unit cell can be embedded in the layer. These inclusions can be separated by a distance $r_i^j \leq d$ and in particular $|x_2^{(j)} - x_2^{(i)}|$ can be less than $R^{(j)} + R^{(i)}$. The interaction between each inclusion of the unit cell cannot be simply accounted for as it was in Ref. 1.

The field in the vicinity of the Jth inclusion is written in the polar coordinate system associated with this inclusion as a sum of a scattered field of coefficient $B_L^{(J)}$ and a locally incident field of coefficient $A_L^{(J)}$

$$p^{[1]}(\mathbf{r}_J) = \sum_{L\in\mathbb{Z}}\left(B_L^{(J)}\mathrm{H}_L^{(1)}\left(k^{[1]}r_J\right) + A_L^{(J)}\mathrm{J}_L\left(k^{[1]}r_J\right)\right)e^{\mathrm{i}L\theta_J}, \tag{10}$$

with $\mathrm{H}_L^{(1)}$ the Lth order Hankel function of the first kind and J_L the Lth order Bessel function and

$$A_L^{(J)} = \sum_{l\in\mathbb{Z}} S_{L-l}B_l^{(J)} + \sum_{j\neq J}\sum_{l\in\mathbb{Z}} S_{L-l}^{(J,j)}B_l^{(j)} + \sum_{j\in\mathcal{N}^c}\sum_{l\in\mathbb{Z}}\sum_{q\in\mathbb{Z}} Q_{qLl}^{(J,j)}B_l^{(j)} + \sum_{n\in\mathcal{N}^i}\sum_{m\in\mathbb{Z}}\sum_{q\in\mathbb{Z}} Z_{qLm}^{(J,n)}D_m^{(n)} + \sum_{q\in\mathbb{Z}} F_{qL}^{(J)},$$

$$F_{Lq}^{(J)} = \frac{2\delta_q\alpha_q^{[0]}}{D_q}\cos\left(k_{2q}^{[1]}x_2^{(J)} - L\theta_q\right)e^{\mathrm{i}k_{1q}^{[1]}x_1^{(J)}},$$

$$S_{L-l} = \sum_{i=1}^{\infty} H_{L-l}^{(1)}\left(k^{[1]}id\right)\left[e^{\mathrm{i}k_1^i id} + (-1)^{L-l}e^{-\mathrm{i}k_1^i id}\right],$$

$$Q_{qLl}^{(J,j)} = \frac{2(-\mathrm{i})^{l-L}e^{\mathrm{i}k_{1q}(x_1^{(J)} - x_1^{(j)})}}{dk_{2p}^{[1]}D_p}\left(\left(\alpha_q^{[1]} - \alpha_q^{[0]}\right)e^{\mathrm{i}k_{2q}^{[1]}H}\cos\left(k_{2q}^{[1]}\left(x_2^{(j)} - x_2^{(J)}\right) - (l-L)\theta_q\right)\right.$$
$$\left. + \alpha_q^{[1]}\cos\left(k_{2q}^{[1]}\left(x_2^{(j)} + x_2^{(J)} - H\right) - (l+L)\theta_q\right) + \mathrm{i}\alpha_q^{[0]}\sin\left(k_{2q}^{[1]}\left(x_2^{(j)} + x_2^{(J)} - H\right) - (l+L)\theta_q\right)\right),$$

$$Z_{qLm}^{(J,n)} = \frac{\mathrm{i}^{L+1}\alpha_{2m}^{[3^{(n)}]}w_n}{dD_p\alpha_q^{[1]}}\sin\left(k_{2m}^{[3^{(n)}]}b_n\right)I_{qm}^{-(n)}e^{\mathrm{i}k_{1q}\left(x_1^{(J)} - d_n + w_n/2\right)}\left(\alpha_q^{[1]}\cos\left(k_{2q}^{[1]}\left(x_2^{(J)} - H\right) - L\theta_q\right) + \mathrm{i}\alpha_q^{[0]}\sin\left(k_{2q}^{[1]}\left(x_2^{(J)} - H\right) - L\theta_q\right)\right), \tag{11}$$

wherein S_{L-l} is the lattice sum often referred to as the Schlömilch series. The terms $S_{L-l}^{(J,j)}$ accounts for the coupling between the multiple inclusions of the unit cell and takes the form

$$S_{Ll}^{(J,j)} = \sum_{q\in\mathbb{Z}} \frac{(-\mathrm{i})^{L-l} 2e^{\pm \mathrm{i}(L-l)\theta_q}}{dk_{2q}^{[1]}} e^{\mathrm{i}\left(k_{1q}(x_1^{(J)}-x_1^{(j)}) \pm k_{2q}^{[1]}(x_2^{(J)}-x_2^{(j)})\right)} \times \left(1-\delta_{Jj}\right), \tag{12}$$

wherein the signs + and − correspond to $x_2^J \geq x_2^j$ and $x_2^J \leq x_2^j$, respectively, which can be found in Ref. 1 when $|x_2^{(J)} - x_2^{(j)}| > R_j + R_i$ or

$$S_{Ll}^{(J,j)} = \mathrm{H}_{L-l}^{(1)}\left(r_J^j\right) e^{\mathrm{i}(l-L)\theta_J^j} + \sum_{o\in\mathbb{Z}} S_{o-l} B_l^{(j)} \mathrm{H}_{L-o}\left(k^{[1]} r_J^j\right) e^{\mathrm{i}(o-L)\theta_J^j}, \tag{13}$$

when $|x_2^{(J)} - x_2^{(j)}| \leq R_j + R_i$. This latter form agrees with the one found in Ref. 21 when the inclusions are aligned inside the unit cell, i.e., $x_2^{(j)} = x_2^{(J)}$, $\forall j \in \mathcal{N}^c$, which imposes $\theta_J^j = 0$ or $\theta_J^j = \pi$. In Eq. (13), (r_J^j, θ_J^j) is the coordinate of $\mathbf{x}^{(j)}$ in the polar coordinate system attached to the Jth inclusions, i.e., centered at $\mathbf{x}^{(J)}$.

Finally, it is well known that the coefficients of the scattered field and those of the locally incident field are linked by a linear relation derived from the boundary condition on $\Gamma_{(J)}$ only, i.e., $B_L^{(J)} = V_L^{(J)} A_L^{(J)}$, wherein $V_L^{(J)}$ are the cylindrical harmonic reflection coefficients. These coefficients take the form $V_L^{(J)} = -\dot{\mathrm{H}}_L^{(1)}(k^{[1]}R_j)/\dot{\mathrm{J}}_L(k^{[1]}R_j)$ in the case of Neumann type boundary conditions, with $\dot{\chi}(x) = d\chi/dx$. Introducing the expression of $A_L^{(J)}$, derived from Eq. (10) in the previous relation, gives rise to the second linear system of equations for the solution of $D_m^{(n)}$ and $B_l^{(j)}$. This second linear system may be written in the matrix form

$$(\mathbf{I} - \mathbf{V}(\mathbf{S}+\mathbf{Q}))\mathbf{B} - \mathbf{VZD} = \mathbf{VF}, \tag{14}$$

wherein $\mathbf{F}$ is a vector of components $\sum_{q\in\mathbb{Z}} F_{Lq}^{(J)}$, which accounts for the solicitation of the Jth inclusion by a wave that is previously diffracted inside the layer, $\mathbf{V}$ is a diagonal square matrix of components $V_L^{(J)}$, $\mathbf{S}$, $\mathbf{Q}$, and $\mathbf{Z}$ are three matrices of components $S_{L-l}\delta_{Jj} + S_{L-l}^{(J,j)}$, which accounts for the direct coupling between the Jth and the jth inclusion, $\sum_{q\in\mathbb{Z}} Q_{Llq}^{(J,j)}$, which accounts for the coupling between the Jth and the jth inclusion through waves diffracted by the layer, and $\sum_{q\in\mathbb{Z}} Z_{Lmq}^{(J,n)}$, which accounts for coupling between the Jth inclusion and the nth irregularity.

C. The linear system of equation for the resolution of $B_l^{(j)}$ and $D_m^{(n)}$ and evaluation of the fields

The final system for the solution of $B_l^{(j)}$ and $D_m^{(n)}$ that gathered Eqs. (8) and (14) reads as

$$\begin{bmatrix} \mathbf{I} - \mathbf{V}(\mathbf{S}+\mathbf{Q}) & -\mathbf{VZ} \\ -\mathcal{Z} & \mathcal{A}-\mathcal{C} \end{bmatrix} \begin{pmatrix} \mathbf{B} \\ \mathbf{D} \end{pmatrix} = \begin{pmatrix} \mathbf{VF} \\ \mathcal{F} \end{pmatrix}. \tag{15}$$

Once this linear system is solved, the expression of R_q in terms of $B_l^{(j)}$ and $D_m^{(n)}$ reads as

$$R_q = \frac{\alpha^{[0]i}\cos\left(k_2^{[1]i}L\right) + \mathrm{i}\alpha^{[1]i}\sin\left(k_2^{[1]i}L\right)}{D^i} + \sum_{q\in\mathbb{Z}}\sum_{j\in\mathcal{N}^c}\sum_{l\in\mathbb{Z}} \frac{4(-\mathrm{i})^l \alpha_q^{[1]}}{dk_{2q}^{[1]} D_q} B_l^{(j)} \cos\left(k_{2q}^{[1]} x_2^{(j)} - l\theta_q\right) e^{-\mathrm{i}k_{1q}x_1^{(j)}} + \sum_{q\in\mathbb{Z}}\sum_{n\in\mathcal{N}^i}\sum_{m=0}^{\infty} \frac{\mathrm{i}w_n e^{\mathrm{i}k_{1p}(d_n - w_n/2)}}{dD_q} D_m^{(n)} \alpha_{2m}^{[3^{(n)}]} \times \sin\left(k_{2m}^{[3^{(n)}]} b_n\right) I_{qm}^{-(n)}. \tag{16}$$

The first term corresponds to the reflection coefficient in absence of inclusions and irregularities of the porous layer with a flat rigid backing. The second terms account for the inclusions. The third term accounts for the irregularities of the rigid backing.

Introduced in Eq. (5), the reflected field is expressed as a sum of (i) the field in the absence of inclusions and irregularities of the rigid backing, (ii) the field due to the inclusions, and (iii) the field due to the irregularities of the rigid backing.

D. Evaluation of the reflection and absorption coefficient

In case of an incident plane wave with spectrum $A^i(\omega)$, the conservation of energy relation takes the form

$$1 = \mathcal{R} + \mathcal{A}, \tag{17}$$

where $\mathcal{R}$ and $\mathcal{A}$ are the hemispherical reflection and the absorption coefficients. $\mathcal{R}$ is defined by

$$\mathcal{R} = \sum_{q\in\mathcal{Z}} \frac{\mathrm{Re}\left(k_{2q}^{[0]}\right)}{k_2^{[0]i}} \frac{\|R_q\|^2}{\|A^i\|^2} = \sum_{q=-\tilde{q}_-}^{\tilde{q}_+} \frac{k_{2q}^{[0]}}{k_2^{[0]i}} \frac{\|R_q\|^2}{\|A^i\|^2}, \tag{18}$$

wherein $\tilde{q}_\mp$ are such that $\tilde{q}_\mp < d/2\pi\left(k^{[0]} \pm k_1^i\right) < \tilde{q}_\mp + 1$ and the expression of R_q are given by Eq. (16). $\mathcal{A}$ takes the form[2,3,7] $\mathcal{A} = \mathcal{A}_D + \mathcal{A}_S$, wherein $\mathcal{A}_D$ is the inner absorption of domains $\Omega^{[1]}$ and $\Omega^{[3^{(n)}]}$, $\forall n \in \mathcal{N}^i$, and $\mathcal{A}_S$ is the surface absorption related to interfaces Γ_H and Γ_n, $\forall n \in \mathcal{N}^i$.

In our calculations, the irregularities are filled with the air medium. Any absorption phenomenon is associated to this material, and thus the inner absorption reduces to the one of domain $\Omega^{[1]}$, and the surface absorption related to Γ_n simplifies.

Because of the complicated shape of $\Omega^{[1]}$ and $\Omega^{[3^{(n)}]}$, and the non-vanishing term $\mathcal{A}_S$, $\mathcal{A}$ will not be calculated by its expression, but rather by $\mathcal{A} = 1 - \mathcal{R}$.

IV. RESULTS AND DISCUSSION

The infinite sum $\sum_{q\in\mathbb{Z}}$ over the indices of the k_{1q} depends on the frequency and on the period of the grating. An empirical truncation rule is employed, inspired from Refs. 1, 2, and 7, and determined by performing a large

TABLE I. Parameters of the porous foam used in the article.

	d (cm)	H (cm)	N^i	b (cm) $\times$ w (cm)	d_n (cm)	N^c	R (cm)	$(x_1^{(j)}\text{cm}, x_2^{(j)}\text{cm})$
C1	8	2	1	3×1	1	3	$R^{(1)}=0.75$	$(x_1^{(1)}, x_2^{(1)}) = (3, 1)$
							$R^{(2)}=0.75$	$(x_1^{(2)}, x_2^{(2)}) = (5, 1)$
							$R^{(3)}=0.75$	$(x_1^{(3)}, x_2^{(3)}) = (7, 1)$
C2	8	3.5	1	3×1	1	6	$R^{(1)}=0.75$	$(x_1^{(1)}, x_2^{(1)}) = (3, 1)$
							$R^{(2)}=0.75$	$(x_1^{(2)}, x_2^{(2)}) = (5, 1)$
							$R^{(3)}=0.75$	$(x_1^{(3)}, x_2^{(3)}) = (7, 1)$
							$R^{(4)}=0.5$	$(x_1^{(2)}, x_2^{(4)}) = (2, 1+\sqrt{3})$
							$R^{(5)}=0.5$	$(x_1^{(3)}, x_2^{(5)}) = (4, 1+\sqrt{3})$
							$R^{(6)}=0.5$	$(x_1^{(3)}, x_2^{(5)}) = (6, 1+\sqrt{3})$
C3	8	2	4	$b^{(1)} \times w^{(1)} = 3 \times 1$	1	3	$R^{(1)}=0.75$	$(x_1^{(1)}, x_2^{(1)}) = (3, 1)$
				$b^{(2)} \times w^{(2)} = 1 \times 0.5$	3		$R^{(2)}=0.75$	$(x_1^{(2)}, x_2^{(2)}) = (5, 1)$
				$b^{(3)} \times w^{(3)} = 1 \times 0.5$	5		$R^{(3)}=0.75$	$(x_1^{(3)}, x_2^{(3)}) = (7, 1)$
				$b^{(4)} \times w^{(4)} = 1 \times 0.5$	7			

number of numerical experiments $\sum_{q=-Q_-}^{Q_+}$ such that $Q_\mp = \text{int}\left(d/2\pi\left(3\text{Re}\left(k^{[1]}\right) \pm k_1^i\right)\right) + 10$. In the latter equations, int(a) represents the integer part of a.

The infinite sum $\sum_{m\in\mathbb{Z}}$ over the indices of the modal representation of the diffracted field by a cylinder is truncated[22] as $\sum_{m=-M}^{M}$ such that $M = \text{int}\,(\text{Re}\,(4.05 \times (k^{[1]}R)^{1/3} + k^{[1]}R)) + 10$.

Finally, the infinite sum (lattice sum) embedded in S_{L-l} in Eqs. (11) and (13) $\sum_{i=1}^{\infty}$ is found to be slowly convergent, particularly in the absence of dissipation, and is found to be strongly dependent on the indice L–l. A large literature exists on this problem.[23,24] Here, the fact that the medium $M^{[1]}$ is dissipative greatly simplifies the evaluation of the Schlömilch series. The superscript I in $S_{L-l}^{\{I\}}$ identifies the integer over which the sum is performed, i.e., $\sum_{i=1}^{I}$. This sum is carried out until the conditions $\left|\text{Re}\left(\left(S_{L-l}^{\{I+1\}} - S_{L-l}^{\{I\}}\right)/S_{L-l}^{\{I\}}\right)\right| \leq 10^{-5}$ and $\left|\text{Im}\left(\left(S_{L-l}^{\{I+1\}} - S_{L-l}^{\{I\}}\right)/S_{L-l}^{\{I\}}\right)\right| \leq 10^{-5}$ are reached.[2]

Numerical calculations have been performed for various geometrical parameters whose values are reported in Table I and within the frequency range of the audible sound, particularly, at low frequencies.

For all calculations, the ambient and saturating fluid is air ($\rho^{[0]} = \rho_f = 1.213\ \text{kgm}^{-3}$, $c^{[0]} = \sqrt{\gamma P_0/\rho_f}$, with $P_0 = 1.01325 \times 10^5\text{Pa}$, $\gamma = 1.4$, and $\eta = 1.839 \times 10^{-5}\text{kgm}^{-3}\,\text{s}^{-1}$). Two of the main constraints in designing acoustically absorbing materials are the size and weight of the configuration. Particular attention is paid to the dimension, i.e., thickness, and the frequencies of the absorption gain, which have to be as small as possible. The absorption gain is defined by reference to the absorption of the same configuration without inclusions embedded and without irregularity of the rigid backing. The initial configuration consists in a $H = 2$ cm thick porous sheet backed by a rigid plate. The material characteristics are reported in Table II and were determined by use of traditional methods.[15,25–27] This material [Fireflex S 309 (b) (Recticel, Wetteren/East-Flanders, Belgium)] presents a large tortuosity for a relatively small flow resistivity. The Biot frequency v_c is also relatively small. The particular phenomena noticed for the different configurations studied therein occur at frequencies higher than v_c. This improves the use of the rigid approximation to model the porous material because the decoupling frequency is always lower than v_c.

TABLE II. Parameters of the porous foam used in the article.

ϕ	α_∞	Λ (μm)	$\Lambda\prime$ (μm)	σ (Ns m^{-4})	v_c (Hz)
0.95	1.42	180	360	8900	781

For the phenomenon related to the inclusions to be large, the filling ratio, i.e., the ratio of the surface occupied by the cylinders $\left[\sum_{j\in\mathcal{N}^c} \pi\left(R^{(j)}\right)^2\right]$ over the total surface of the layer inside the unit cell ($d \times H$), has to be large. This also implies the use of large radius inclusions and therefore the use of a large thickness layer. The absorption coefficient associated with the layer can be larger than the one associated with the periodic inclusions in this latter case. This leads to compromises between radius of the inclusions and the layer thickness, as stated in Ref. 3.

One array of circular cylinders will be considered as the first step, i.e., $d^c \leq d$, for the layer thickness and so for the global system thickness to be as small as possible. Inspired by the configuration studied in Ref. 3, circular cylinder of 7.5 mm radius, whose center x_2-coordinate are $x_2^{(j)} = H/2 = 1$ cm, are embedded with a spatial periodicity of $d^c = 2$ cm. The fundamental modified mode of the plate associated with d^c stands around $v_{(1,1)}^c = 15$ kHz at normal incidence, the fundamental Bragg frequency (associated with $x_2^{(j)}$) stands around $v_b = 6$ kHz, while the complex trapped mode (CTM) stands below the quarter-wavelength resonance frequency around $v_t^c = 2400$ Hz. [3]

Irregularities of the rigid backing are also added to increase the absorption below the frequency of the fundamental CTM and/or around the fundamental Bragg frequency. In Ref. 7, a low resistivity rigid porous sheet was used for the MMBL associated with the global period d to be correctly excited. Effectively, for them to be excited, the associated waves, which are propagative in the layer and evanescent in the semi-infinite domain, should be able to correctly propagate inside the layer. The presence of the inclusions partly blocks their propagation. Therefore, the associated absorption cannot be close to unity when

inclusions are embedded. Nevertheless, it was shown that a quasi-total absorption peak can be obtained at the frequency of the fundamental resonance of the irregularity, when the latter stands below the frequency of the fundamental associated modified mode of the plate.[7] The followed phenomena are then closer to Schröeder scatterers.[8,28]

The periodicity of the global configuration is determined by the periodicity of the irregular backing. The unit cell contains at least one irregularity per spatial period and at least one inclusion. The mode associated with the global periodicity is studied in the Appendix.

A. Single irregularity and more than one inclusion per spatial period

In most of the studies related to irregular rigid grating associated with a layer, MMBL and mode of the irregularity (MI) were chosen to stand either largely below or largely above the quarter-wavelength resonance. The latter resonance is not a real mode but a leaky mode due to interference phenomena.[7,29] Despite the fact that the irregular grating was assumed to excite the real mode of the plate, i.e., Pekeris or Love modes, whose frequencies are usually shifted below the quarter-wavelength resonance frequency, the irregularity was not designed for its fundamental quasi-mode frequency to stand close to the quarter-wavelength resonance frequency. In absence of inclusion, for a fixed layer thickness H and irregularity width w, geometrical parameters d and b exist for which a trapped mode associated with the irregularity (TMI) exists and can be excited. The latter can be either understood as a trapped mode, whose structure is close to the fundamental quasi-mode of the irregularity, i.e., plane wave inside the irregularity that mainly radiates waves inside the layer or as a coupled MI together with the quarter-wavelength resonance. The excitation of the TMI is weakly dependent upon the angle of incidence of the solicitation, which means that the TMI is closer to the MI. Effectively the latter does not depend on the incidence angle of the solicitation.

For $d=8$ cm and a $b \times w = 3$ cm $\times$ 1 cm irregularity, such a mode exists. The fundamental MI is excited at $\nu_{(0,0)}^{(MI)} = c^{[3]}/4b = 2850$ Hz, while the trapped mode (TMI) is excited around $\nu_t^{(i)} = 2000$ Hz, Fig. 2 The associated fundamental MMBL frequency is $\nu_{(1,1)}^{(i)} = 3800$ Hz at normal incidence.

For the TMI to be excited, i.e., to be correctly coupled with the incident waves, the plate area just above the irregularity must be free of inclusion. This would effectively block waves traveling from the semi-infinite domain toward the irregularity. The final dimensions of the configuration C1 are reported in Table I.

Figure 3 depicts the absorption coefficient of the configuration C1, when solicited at normal incidence. From the high frequency bound to the low frequency one, the peak around 8500 Hz corresponds to the second MI $\nu_{(1,0)}^{(MI)} = 3c^{[3]}/4b = 8550$ Hz. The latter frequency effectively corresponds to a zero of the pressure field in the middle of the bottom segment of the irregularity, Fig. 4(a). The absorption minimum is centered at the first Bragg frequency,

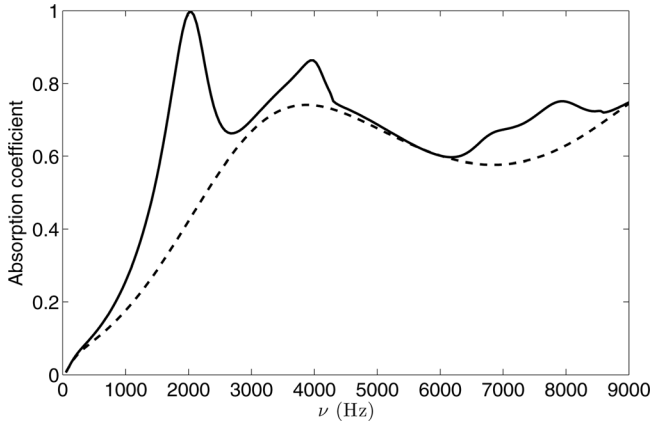

FIG. 2. Absorption coefficient of a $H=2$ cm thick porous sheet of Fireflex backed by a rigid flat plate (– – –) without inclusion and irregularity of the rigid backing and (—) with an irregularity, $b \times w = 3$ cm $\times$ 1 cm, per spatial period $d=8$ cm of the rigid backing. The TMI is excited around $\nu_t^{(i)} = 2000$ Hz.

$\nu_b = \mathrm{Re}\left(c^{[1]}\right)/4x_2^{(1)} \approx 6000$ Hz. The latter frequency corresponds to the frequency at which the two circular gratings, i.e., the real grating and its image with respect to the Neumann type boundary condition Γ_0 interfere. The peak around $\nu_{(1,1)}^{(i)} = 3500$ Hz is the fundamental MMBL associated with d. The field, Fig. 4, at this frequency is mainly composed of evanescent waves in the air medium and propagative ones in the porous sheet. This peak does not correspond to a total absorption because the waves associated with this mode are hindered by the presence of the circular inclusions inside the porous sheet. The peak around $\nu_t^{(c)} = 3000$ Hz is associated with the degenerated CTM linked to the three inclusions whose center-to-center distance is 2 cm. This CTM is degenerated because one inclusion is missing for the periodicity of the cylinder arrangement to be $d^{(c)}=2$ cm. Finally, the total absorption peak, around $\nu_t^{(i)} = 1800$ Hz, is associated with the trapped mode linked to the irregularity.

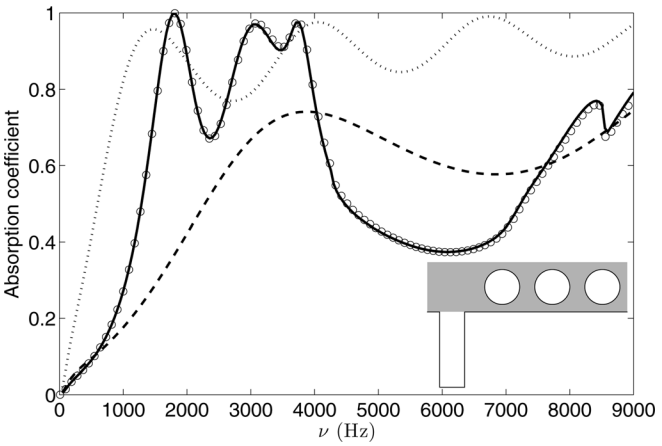

FIG. 3. Configuration C1—absorption coefficient of a porous sheet of Fireflex backed by a rigid flat plate, when the thickness is $H=2$ cm (– – –) and when the thickness is $H+b=5$ cm (· · ·) without inclusion embedded and (—) with three $R=75$ mm radius circular cylinders embedded per spatial period $d=8$ cm, with an irregularity of the rigid backing. The finite element result is plotted with (○).

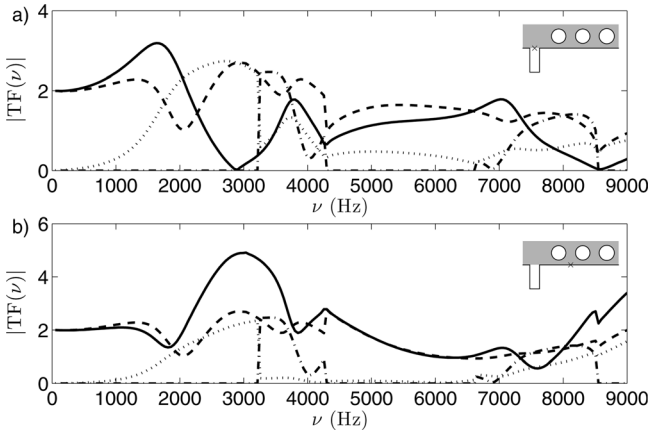

FIG. 4. Configuration C1—transfer function TF (—) on Γ_0 (a) at the center of the bottom segment of the irregularity, i.e., $x_1 = 1$ cm and (b) in the middle of the unit cell, i.e., $x_1 = 4$ cm, and its different components: $\mathrm{TF}_1(\nu)$, propagative waves in both $\Omega^{[0]}$ and $\Omega^{[1]}$ ($\cdots$); $\mathrm{TF}_2(\nu)$, propagative waves in $\Omega^{[0]}$ and evanescent waves in $\Omega^{[1]}$ ($-\cdot-\cdot$); and $\mathrm{TF}_3(\nu)$, evanescent waves in both $\Omega^{[0]}$ and $\Omega^{[1]}$ ($\cdots$).

The absorption is compared, Fig. 3, with a $H = 2$ cm thick foam plate, i.e., the initial thickness of the porous plate employed in the global structure without inclusion and without irregularity of the rigid backing, and with a $H + b = 5$ cm thick foam plate, which corresponds to a homogeneous porous plate of the same thickness as the global final configuration. The absorption coefficient for the $H + b = 5$ cm thick foam plate is, on the average, higher than the absorption coefficients of the other two configurations over the frequency range, but any total or quasi-total absorption peaks are noticed. Moreover, the total amount of foam material is lower when inclusions and irregularities are considered and the dimensions of the global configuration are less than $H + b$. In what follows, the absorption coefficient is compared with the one for the initial porous plate of thickness H.

The snapshots of the pressure field inside the porous sheet and the irregularity are depicted in Fig. 5. From this figure, it becomes clear that both absorption peaks at $\nu_t^{(i)}$ and $\nu_t^{(c)}$ are related to trapped mode excitation of the irregularity and three cylinders set, respectively.

The numerical validation was performed by matching the absorption coefficient, as calculated with the present method, with the one as calculated with a finite element method. A pressure variational formulation is discretized by quadratic finite elements inside the unit cell, thereby leading to a discretized problem of 2303 elements and 1327 nodes. The periodicity relation, i.e., the Floquet condition, was applied on both sides of the discretized domain, i.e., at each nodes of the x_1-coordinate 0 and d. For this periodicity relation to be correctly implemented, the meshes of these two sides should have similar nodes, i.e., identical x_2-coordinate. The results match well, thus validating the described method, Fig. 3. Note that the finite element result is slightly more rigid (i.e., the frequencies are higher), which is a classical result. The small discrepancy close to the high frequency bound can be enhanced by a mesh refinement.

The width of the irregularity mainly influences the frequencies $\nu_t^{(i)}$ and $\nu_{(1,1)}$. When w is varied (from 5 mm to 20 mm) over a range that does not lead to an overlapping of the irregularity and of the cylinders, both $\nu_t^{(i)}$ and $\nu_{(1,1)}$ decrease, while the amplitude of the associated peaks remains constant. The cylinder radius acts on both $\nu_t^{(c)}$, which decreases when $R^{(j)}$, $j \in \mathcal{N}^c$ increases, and the amplitude of the absorption at this frequency. For smaller radii, the degenerated CTM strongly interferes with the fundamental MMBL, creating a peak of amplitude close to unity over a possibly relatively large frequency band. The amplitude of the peak possesses a maximum value when the radius increases and then drastically decreases because the wave can no longer propagate toward the rigid backing. The radius for which the amplitude is maximum is $R^{(j)} = 7.5$ mm.

When the angle of incidence varies, the frequency and amplitude of the trapped mode linked to the irregularity are not modified. In addition, $\nu_{(1,1)}$ decreases and the amplitude of the associated peak increases. $\nu_t^{(c)}$ decreases until $\nu_{(1,1)}$ becomes lower than $\nu_t^{(c)}$, leading to a disappearance of the peak associated with the trapped mode connected to the inclusions. In fact, this mode and the fundamental modified mode of the plate become coupled mode.

Because the parameters of a foam are often difficult to predict before its polymerization, a sensitivity analysis has been performed with regards to the acoustic and structural parameters of the porous sheet. Each parameter of the porous foam is varied one after the other, while keeping the other constant at their value as shown in Table II. Each parameter

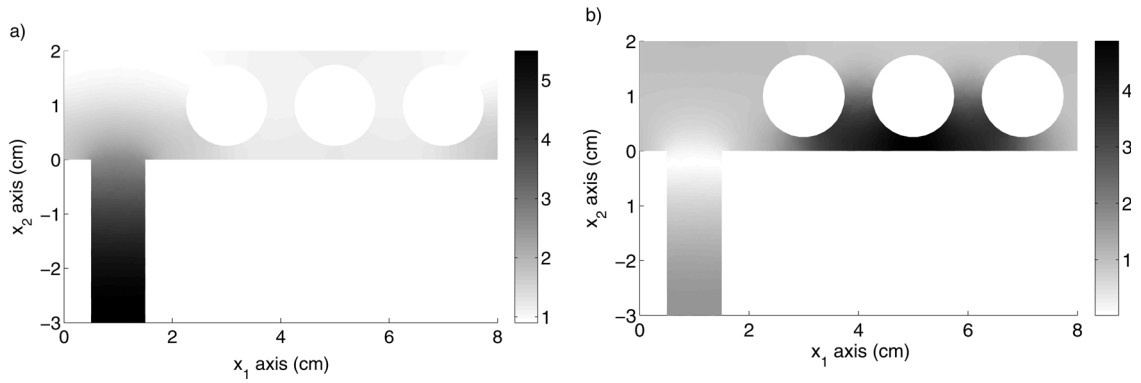

FIG. 5. Configuration C1—snapshots of the pressure field in the porous sheet and the irregularity of the unit cell (a) at $\nu_t^{(i)} = 1810$ Hz and (b) $\nu_t^{(c)} = 3070$ Hz.

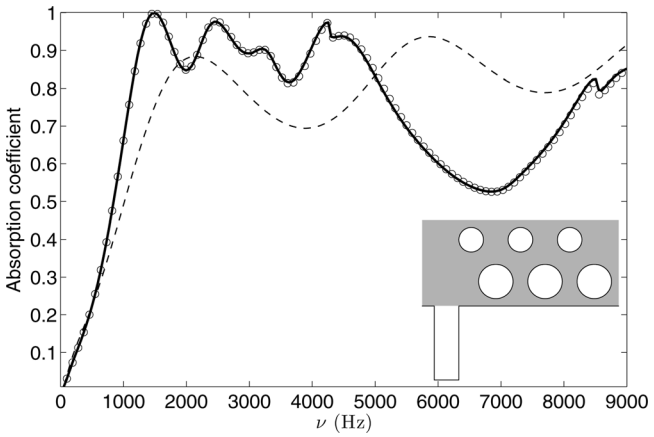

FIG. 6. Configuration C2—absorption coefficient of a $H=3.5$ cm thick porous sheet of Fireflex backed by a rigid flat plate ($---$) without inclusion embedded and (—) with three $R=75$ mm and three $R=5$ mm radius circular cylinders embedded per spatial period $d=8$ cm, with an irregularity of the rigid backing. The finite element result is plotted with (○): discretized problem of 5724 elements and 3135 nodes.

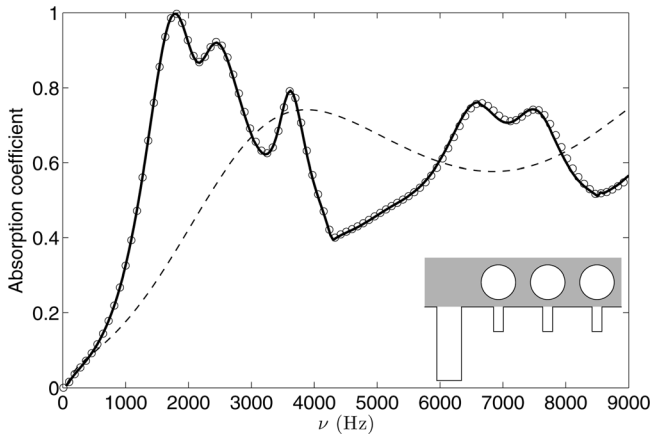

FIG. 7. Configuration C3—absorption coefficient of a $H=2$ cm thick porous sheet of Fireflex backed by a rigid flat plate without inclusion embedded ($---$) and (—) with three circular cylinders embedded and four irregularities of the rigid backing per spatial period $d=8$ cm. The finite element result is plotted with (○): descritized problem of 3154 elements and 1784 nodes.

is assumed to be independent from the other, but their variations correspond to those encountered in practice. The amplitude and frequency of the absorption peaks are quasi-independent from a variation of ϕ, Λ, and Λ'. The amplitude of the TMI, MMBLI, and CTM are quite independent from a variation of α. On the other hand, while both frequencies $v_t^{(i)}$ and $v_{(1,1)}$ slowly decrease when α increases from 1.02 to 1.42, $v_t^{(c)}$ largely decreases. The resistivity σ $(2900\ \text{Ns m}^{-4}; 13900\ \text{Ns m}^{-4})$ has a large influence on the amplitude of the CTM but not on the amplitude of the other peaks. When the resistivity increases, the amplitude decreases, and the peak is wider, while $v_t^{(c)}$ increases. Everything seems to happen as if the material properties of the porous sheet mainly influences the phenomena associated with the cylinders, while the influence of these parameters on those associated with the irregularity are hidden by the influence of the cylinders.

The addition of a second grating of inclusions, leading to an increase of the layer thickness that is still acceptable, enables the interactions of the different modes. Figure 6 depicts the absorption coefficient for the configuration C2. This configuration is derived from Ref. 3 and consists of a modification of a triangular lattice by reducing the radius of the second row of inclusions and removing the fourth pattern of inclusion just below the irregularity. The absorption coefficient is largely increased in the frequency range between the two CTMs associated with the inclusions,[3] $v_t^{(c)} \approx 1500$ Hz and $v_t^{(c)} \approx 4000$ Hz. This results from a complex combination of the two trapped modes, the fundamental MI and the MMBL. The influence of the angle of incidence is quite similar to that of the absorption coefficient of the configuration C1. Nevertheless, the absorption linked to the porous sheet is already large and the addition of a row of inclusions would be of no practical use. The method is validated by matching the absorption coefficient calculated with the present method with the one calculated from the finite element method, Fig. 6.

B. More than one irregularity and more than one inclusion per spatial period

The configuration C1 becomes more complex by adding irregularities.

The addition of a higher irregularity, whose fundamental MI would stand below the previous one and below the MMBL, is of no practical use. Effectively, despite the fact that such irregularity usually leads to an absorption coefficient close to unity for a frequency close to its fundamental MI,[7] the height that should be used is too large for the purpose of this work. For example, for an absorption peak to stand at 1 kHz, a $b^{(2)} = 4c^{[3]}/1 \times 10^3 = 8$ cm irregularity should be added. The total thickness of the sample is therefore 10 cm. It is then obvious that the first irregularity has to be the highest irregularity of the system.

Three identical irregularities $b^{(j)} \times w^{(j)} = 1\ \text{cm} \times 5\ \text{mm}$, $j=2, 4$ were added to the configuration C1. These were equally spaced at $d_i^j = 2$ cm, $i \neq j$. Figure 7 depicts the absorption coefficient of this structure when the configuration is solicited by a normal incident plane wave. The frequency of the fundamental mode of the additional irregularities is $v_{(0,0)}^{MI} = 8500$ Hz. The fundamental mode of these additional irregularities interacts with the second mode of the first irregularity. This interaction leads to coupled modes that trap more energy. The translation of the excitation of these two modes is the two peaks of absorption between 6000 and 8000 Hz, i.e., inside frequency range of the initial minimum of absorption. The frequency of the trapped mode associated with the circular cylinders is lower because the apparent distance from the center of the inclusions to the bottom of the irregularity is larger than $x_2^{(j)}$. In Ref. 3, it was found that $v_t^{(c)}$ decreases when $x_2^{(j)}$ increases. The addition of these three irregularities leads to a decrease in the amplitude of the peak associated with the excitation of the fundamental MMBL. This can be partly explained by the fact that the associated waves can stand with difficulty because of the more irregular backing

and by the fact that the period is now closer to $d=2$ cm than it was for the configuration C1. The increase of the absorption coefficient is less than it was in the configuration C1 between 1000 and 4000 Hz, but the absorption largely increases between 6000 and 8000 Hz. The method is validated by matching the absorption coefficient calculated with the present method with the one calculated with the finite element method, Fig. 7.

V. CONCLUSION

The combined influence of embedding periodic circular rigid inclusions on the absorption of a rigid frame porous sheet and of periodic irregularities of the rigid plate on which the structure is attached was studied theoretically and numerically. In addition to the absorption features related to the Bragg interference and to the modified mode of the layer, it has been shown that the structure, in the case of one irregularity and one multi-inclusions array embedded in the porous sheet per spatial period, possesses absorption peaks close to and below the quarter-wavelength resonance of the sheet, when the dimension and parameters of the material are correctly chosen. These peaks are associated with trapped modes connected to the presence of the inclusion and irregularity. In particular, it is shown that the absorption peak associated with the irregularity is quasi-total and quasi-independent of the angle of incidence. This particular feature enables the design of small dimension absorption packages. This absorption peak was validated by use of finite element method, thus validating the described method and accuracy of the predicted results.

The addition of the inclusions array increases the number of absorption peaks connected to the inclusion but rapidly leads to large thickness structures. The embedding of the additional inclusions becomes useless. The addition of smaller size irregularities leads to an increase of the absorption around the Bragg interference frequencies without increasing the total thickness of the sample.

The method offers a quite efficient alternative to multilayering and double porosity materials for the design of sound packages. Optimization of the parameters and dimensions should now be achieved in order to find the optimal configuration depending on the frequency range on which the absorption coefficient should be increased. The latter optimization procedure would be constrained, notably by the dimensions and weight of the structure which have to be as small as possible.

ACKNOWLEDGMENT

The authors would like to thank Matthew Boucher for his useful help during the writing of the article.

APPENDIX: MODAL ANALYSIS OF THE CONFIGURATION

The modes of the configuration without embedded inclusions (i.e., a rigid porous layer backed with a planar rigid wall), whose dispersion relation is

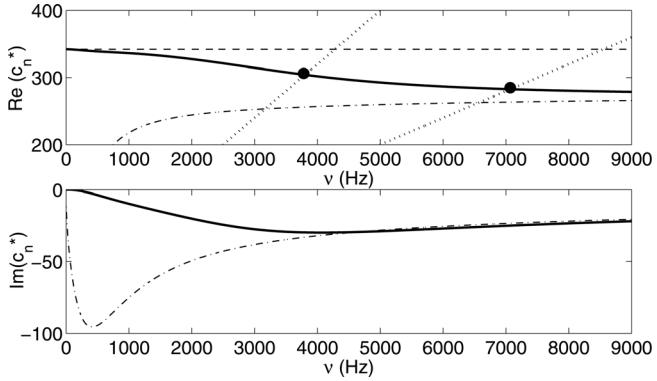

FIG. 8. Real and imaginary part of the root of the dispersion relation in absence of inclusions $c^{\star}_{(n)}$, $n=1$, 2. Real part of the MMBL $c^{\star}_{(n,q)}$, $n=1$, 2, $q=1$, 2, for $d=8$ cm are pointed out by dot.

$$D^i = \alpha^{[0]i}\cos\left(k_2^{[1]i}H\right) - \mathrm{i}\alpha^{[1]i}\sin\left(k_2^{[1]i}H\right) = 0 \qquad \text{(A1)}$$

cannot be excited by a plane incident wave initially traveling in the air medium.[7] Effectively, Fig. 8 depicts the real and the imaginary parts of the roots $c^{\star}_{(n)}(\omega) = \omega/k^{\star}_{1,(n)}(\omega)$ of Eq. (A1), as calculated for a $H=2$ cm thick porous layer, whose acoustical characteristics are those used in Sec. IV. Under the rigid frame assumption and for frequencies higher than the Biot frequency (but lower than the diffusion limit), a porous material can be considered as a modified fluid, its associated dissipation being considered as a perturbation of a fluid. For Eq. (A1) to be true without dissipation, $k_2^{[0]}$ should be purely imaginary while $k_2^{[1]}$ should be purely real. Under the previous assumptions, this implies that $\mathrm{Re}\left(c^{\star}_{(n)}\right)$ should lie in $[\mathrm{Re}(c^{[1]}), c^{[0]}]$, i.e., $|k_1^i|$ should lie in $[k^{[0]}; \mathrm{Re}(k^{[1]})]$, or for a plane incident wave initially propagating in the air medium, $|k_1^i|$ is always smaller than $k^{[0]}$. It is also necessary to note that in the diffusion regime, i.e., for frequencies much lower than the Biot Frequency, no mode exists. This fact constitutes the major difference when compared with a traditional fluid. Effectively, for frequencies much lower than the Biot frequency, $k^{[1]}$ is purely imaginary. This implies that $k_{2_i}^{[1]}$ is also purely imaginary for all the values of k_1^i and that D never vanishes.

When inclusions are periodically embedded in the porous sheet and irregularities are periodically added to the rigid backing, the dispersion relation of the modes of the configuration is

$$\det\begin{pmatrix} \mathbf{I} - \mathbf{V}(\mathbf{S}+\mathbf{Q}) & -\mathbf{V}\mathbf{Z} \\ -\mathcal{Z} & \mathcal{A}-\mathcal{C} \end{pmatrix} = 0. \qquad \text{(A2)}$$

Here, we focus on the case of only one cylinder and irregular grating, i.e., $N^c=1$ and $N^i=1$, in order to emphasize the excitation of the MMBL. Proceeding as in Ref. 2, an iterative scheme can be employed to solve Eq. (15). The equations are re-written in the form $(1-V_L M_{LL})B_L = V_L F_L + V_L \sum_{l\in\mathbb{Z}} M_{Ll}B_l(1-\delta_{Ll}) + V_L \sum_{m\in\mathbb{Z}} Z_{Lm}D_m$ and $(\mathcal{A}_M - \mathcal{C}_{MM})D_M = \mathcal{F}_M + \sum_{m\in\mathbb{Z}} \mathcal{C}_{Mm}D_m(1-\delta_{Mm}) + \sum_{l\in\mathbb{Z}} \mathcal{Z}_{Ml}B_l$. The iterative scheme reads as

$$\begin{cases} B_L^{\{0\}} = V_L F_L/(1 - V_L M_{LL}) \\ B_L^{\{n+1\}} = \left(V_L \sum\limits_{l\in\mathbb{Z}} M_{Ll} B_l^{\{n\}} (1 - \delta Ll) + V_L \sum\limits_{m\in\mathbb{Z}} Z_{Lm} D_m^{\{n\}} + V_L F_L \right) \Big/ (1 - V_L M_{LL}) \\ \\ D_L^{\{0\}} = \mathcal{F}_M/(\mathcal{A}_M - \mathcal{C}_{MM}) \\ D_L^{\{n+1\}} = \left(\mathcal{F}_M + \sum\limits_{m\in\mathbb{Z}} \mathcal{C}_{Mm} D_m^{\{n\}} (1 - \delta_{Mm}) + \sum\limits_{l\in\mathbb{Z}} \mathcal{Z}_{Ml} B_l^{\{n\}} \right) \Big/ (\mathcal{A}_M - \mathcal{C}_{MM}) \end{cases}, \tag{A3}$$

from which it becomes apparent that the solutions $B_L^{\{n\}}$ and $D_M^{\{n\}}$, to any order of approximation, are expressed as a fraction. The denominator of which, being independent of the order of approximation, can become small for certain couples (k_{1q}, ω), so as to make $B_L^{\{n\}}$ and $D_M^{\{n\}}$, maybe even the field large. Moreover, after the first iteration, it becomes apparent that the denominator of both $B_L^{\{J\}}$ and $D_M^{\{N\}}$ becomes $(1 - V_L M_{LL})(\mathcal{A}_M - \mathcal{C}_{MM})$. When this denominator is small, the field is possibly large.

When this happens, a natural mode of the configuration, comprised of the inclusions, the irregular backing and the layer, is excited, thus taking the form of a resonance with respect to $B_L^{\{n\}}$ and $D_M^{\{n\}}$. As $B_L^{\{n\}}$ and $D_M^{\{n\}}$ are related to f_p, g_p, and R_p, the structural resonance manifests itself for the same (k_{1q}, ω), in the fields of the layer and in the air.

The approximate dispersion relation is

$$\mathcal{D}_L = \left(1 - V_L \left(S_0 + \sum_{q\in\mathbb{Z}} Q_{qLL}\right)\right)\left(\mathcal{A}_M - \sum_{q\in\mathbb{Z}} \mathcal{C}_{qMM}\right) = 0. \tag{A4}$$

This equation is satisfied when either $1 - V_L\left(S_0 + \sum_{q\in\mathbb{Z}} Q_{qLL}\right) = 0$ or $\mathcal{A}_M - \sum_{q\in\mathbb{Z}} \mathcal{C}_{qMM} = 0$. Both these equations[3,7] are satisfied when $|k_{1q}| \in [k^{[0]}, \mathrm{Re}(k^{[1]})]$ and when either $D_q = 0$ or $\alpha_q^{[1]} = 0$ (i.e., $k_{2q}^{[1]} = 0$), which, respectively, corresponds to the modified modes of the backed layer (MMBL) and to the modes of the grating (MG). Both of them are determined by the intersection of $c_{1q} = \omega/k_{1q}$, respectively, with $c_{(n)}^{\star}(\omega)$ as calculated for the backed layer and with $\mathrm{Re}(c^{[1]})$. The MMBL are pointed out by the dots on Fig. 8. The associated attenuation of each mode can then be determined by the values of $\mathrm{Im}\left(c_{(n)}^{*}\right)$ and Im $(c^{[1]})$ at the frequencies at which the modes are excited. The attenuation associated with MG is also higher than the one associated with MMBL for all frequencies. Moreover, MG corresponds to the highest boundary of $|k_{1q}|$ for Eq. (A4) to be true. This implies that MG should be difficult to excite. This type of mode can only be poorly excited by a plane incident wave, particularly, at low frequencies.

[1]J.-P. Groby, E. Ogam, and A. Wirgin, "Acoustic response of a periodic distribution of macroscopic inclusions within a rigid frame porous plate," Waves Random Complex Media **18**, 409–433 (2008).
[2]J.-P. Groby, A. Wirgin, L. De Ryck, W. Lauriks, Y. Xu, and R. Gilbert, "Acoustic response of a rigid-frame porous medium plate with a periodic set of inclusions," J. Acoust. Soc. Am. **126**, 685–693 (2009).
[3]J.-P. Groby, O. Dazel, A. Duclos, L. Boeckx, and W. Lauriks, "Quasi-total absorption peak by use of a backed rigid frame porous layer with circular periodic inclusions embedded," ArXiv:physics/1007.3177 (2010).
[4]V. Tournat, V. Pagneux, D. Lafarge, and L. Jaouen, "Multiple scattering of acoustic waves and porous absorbing media," Phys. Rev. E **70**, 026609 (2004).
[5]E. Gourdon and M. Seppi, "On the use of porous inclusions to improve the acoustical response of porous materials: Analytical model and experimental verification," Appl. Acoust. **71**, 283–298 (2010).
[6]X. Olny and C. Boutin, "Acoustic wave propagation in double porosity media," J. Acoust. Soc. Am. **114**, 73–89 (2003).
[7]J.-P. Groby, W. Lauriks, and T. Vigran, "Total absorption peak by use of a rigid frame porous layer backed by a rigid multi-irregularities grating," J. Acoust. Soc. Am. **127**, 2865–2874 (2010).
[8]M. R. Schröeder, "Toward better acoustics for concert halls," Phys. Today **33**, 24–30 (1980).
[9]B. Sapoval, B. Hebert, and S. Russ, "Experimental study of a fractal acoustical cavity," J. Acoust. Soc. Am. **105**, 2014–2019 (1999).
[10]B. Sapoval, S. Felix, and M. Filoche, "Localisation and damping in resonators with complex geometry," Eur. Phys. J. Spec. Top. **161**, 225–232 (2008).
[11]T. Utsunomiya and R. Eatock Taylor, "Trapped modes around a row of circular cylinders in a channel," J. Fluid Mech. **386**, 259–279 (1999).
[12]R. Porter and D. V. Evans, "Rayleigh–Bloch surface waves along periodic gratings and their connection with trapped modes in waveguides," J. Fluid Mech. **386**, 233–258 (1999).
[13]R. Porter and D. Evans, "Embedded Rayleigh–Bloch surface waves along periodic rectangular arrays," Wave Motion **43**, 29–50 (2005).
[14]C. Linton and P. McIver, "Embedded trapped modes in water waves and acoustics," Wave Motion **45**, 16–29 (2007).
[15]J.-F. Allard and N. Atalla, *Propagation of Sound in Porous Media: Modelling Sound Absorbing Materials* (Wiley, Chichester, 2009), Chap. 5, pp. 73–107.
[16]L. De. Ryck, J.-P. Groby, P. Leclaire, W. Lauriks, A. Wirgin, C. Depollier, and Z. Fellah, "Acoustic wave propagation in a macroscopically inhomogeneous porous medium saturated by a fluid," Appl. Phys. Lett. **90**, 181901 (2007).
[17]J.-F. Allard and Y. Champoux, "New empirical equations for sound propagation in rigid frame fibrous materials," J. Acoust. Soc. Am. **91**, 3346–3353 (1992).
[18]D. Johnson, J. Koplik, and R. Dashen, "Theory of dynamic permeability and tortuosity in fluid-saturated porous media," J. Fluid Mech. **176**, 379–402 (1987).
[19]J.-P. Groby and A. Wirgin, "Seismic motion in urban sites consisting of blocks in welded contact with a soft layer overlying a hard half space," Geophys. J. Int. **172**, 725–758 (2008).
[20]S. Wilcox, L. C. Botten, R. C. McPhedran, C. G. Poulton, and C. Martijin de Sterke, "Modeling of defect modes in photonic crystals using the fictitious source superposition method," Phys. Rev. E **71**, 056606 (2005).
[21]L. C. Botten, N.-A. P. Nicorovici, A. A. Asatryan, R. C. McPhedran, C. Poulton, C. Martijin de Sterke, and P. A. Robinson, "Formulation for electromagnetic scattering and propagation through grating stacks of metallic and dielectric cylinders for photonic crystal calculations. Part I. Method," J. Opt. Soc. Am. A **17**, 2165–2176 (2000).
[22]P. Barber and S. Hill, "Light scattering by particles: Computation methods," in *Advanced Series in Applied Physics 2* (Wolrd Scientific Publishing Co. Pte. Ltd., London, 1990), Chap. 2, p. 30.

[23]V. Twersky, "On scattering of waves by the infinite grating of circular cylinders," IRE Trans. Antennas Propag. **10**, 737–765 (1962).
[24]C. M. Linton, "Schlomilch series that arise in diffraction theory and their efficient computation," J. Phys. A: Math. Gen. **39**, 3325–3339 (2006).
[25]R. Brown and R. Bolt, "The measurement of flow resistance of porous acoustic materials," J. Acoustc. Soc. Am. **13**, 337–344 (1942).
[26]Ph. Leclaire, L. Kelders, W. Lauriks, N. Brown, M. Melon, and B. Castagnède, "Determination of the viscous and thermal characteristic lengths of plastic foams by ultrasonic measurements in helium and air," J. Appl. Phys. **80**, 2009–2012 (1996).
[27]Z. E. A. Fellah, F. G. Mitri, M. Fellah, E. Ogam, and C. Depollier, "Ultrasonic characterization of porous materials: Inverse problem," J. Sound Vib. **302**, 746–759 (2007).
[28]T. Wu, T. J. Cox, and Y. W. Lam, "From a profiled diffuser to an optimized absorber," J. Acoust. Soc. Am. **108**, 643–650 (2000).
[29]N. Haskell, "The dispersion of surface waves in multilayered media," Bull. Seismol. Soc. Am. **43**, 17–34 (1953).